COBEM 2023 27TH INTERNATIONAL CONGRESS OF MECHANICAL ENGENEERING

ABCM Brazilian Society of Mechanical Sciences and Engineering
27th ABCM International Congress of Mechanical Engineering
December 04-08, 2023, Florianópolis-SC, Brazil

COB-2023-0112
THE ENRICHED MODIFIED LOCAL GREEN'S FUNCTION METHOD APPLIED TO STATIC CRACKS

Ramon Macedo Corrêa
Marcos Arndt
Roberto Dalledone Machado
Graduated Program in Civil Engineering - Federal University of Paraná
ramon.correa@ufpr.br
arndt@ufpr.br
rdm@ufpr.br

Abstract. *The Modified Local Green's Function Method (MLGFM) is an integral method that can be understood as a hybrid of the Boundary Element Method and the Finite Element Method. The paper proposes to bring enrichment techniques based on the Generalized Finite Element Method to the MLGFM context. This enriched version of the MLGFM is applied to static cracks. Two examples are presented and the results are compared to the Generalized Finite Element Method ones.*

Keywords: *Green's Functions, Generalized Finite Element Method, Boundary Element Method, Fracture Mechanics*

1. INTRODUCTION

The Modified Local Green's Function Method (MLGFM) is an integral method developed, firstly, by Barcellos and Silva (1987) based on Burns (1975), Horak and Dorning (1977), and Horak (1980) ideas of obtaining discrete projections of the Green Functions. In the original proposal, the MLGFM used the Finite Element Method (FEM) (Bathe, 1996; Zienkiewicz *et al.*, 2005) to obtain these discrete projections in order to use them as a fundamental solution in the Boundary Element Method (BEM) formulation (Brebbia *et al.*, 1984; Brebbia and Dominguez, 1992), so, the MLGFM can be understood as a hybrid of the FEM and BEM.

The MLGFM does not require an explicit fundamental solution or a Green's function, since the method uses a projection of the Green's function determined by the FEM technique. Consequently, it can be applied to problems that lack a known fundamental solution. The method demonstrates superconvergence characteristics regarding nodal values related to tractions and displacements.

The mathematical background of the original MLGFM was formally presented in Barbieri *et al.* (1998), where the formulation can be found with details. Since its proposal, the MLGFM was applied to several solid mechanics problems, see for instance: Barbieri and Barcellos (1993a), Barbieri and Barcellos (1993b), Machado *et al.* (1994), Barbieri and Muñoz (1998), Machado *et al.* (2008), and Barbieri and Machado (2015).

The Generalized Finite Element Method (GFEM) originated in an idea presented by Babuška *et al.* (1994), where the authors proposed a "Special finite element" that generates its shape functions multiplying a function by a "*hat function*". Latter, Melenk (1995) showed that these "*hat*" functions can be replaced by any partition of unity function. Babuška and Banerjee (2012) proposed slightly modifying the enrichment functions to bring more numerical stability to the method.

Over the years, the main application of GFEM has been in fracture mechanics, as can be seen in Dolbow *et al.* (2000), Kim *et al.* (2011), Gupta *et al.* (2012), Rivadeneira and Duarte (2019), among several other works. In this paper, the proposal is to bring the GFEM ideas to the MLGFM and apply them to fracture mechanics problems.

2. MODIFIED LOCAL GREEN'S FUNCTION METHOD FORMULATION

This MLGFM formulation is based on a new approach first presented by the authors in Corrêa *et al.* (2023). For a general elastic problem, the following boundary value problem arises:

$$\nabla \cdot \boldsymbol{\sigma} = \mathbf{b} \quad \text{in} \quad \Omega, \tag{1}$$

where $\boldsymbol{\sigma}$ is the stress tensor, $\mathbf{b}$ are the body forces, and ∇ is the gradient operator, with the following boundary conditions:

$$\mathbf{u} = \bar{\mathbf{u}} \quad \text{in} \quad \Gamma_{\mathrm{D}}, \tag{2}$$

and

$$\boldsymbol{\sigma} \cdot \mathbf{n} = \bar{\mathbf{t}} \quad \text{in} \quad \Gamma_{\mathrm{N}}, \tag{3}$$

where $\mathbf{n}$ is the normal vector to the boundary, $\mathbf{t}$ are the boundary reactions, and Γ_{D} and Γ_{N} are the Dirichlet and Neumann boundaries, respectively.

Applying the weighted residual method over the domain using $\mathbf{w}$ as a weight function, and applying the Green's theorem, the following equations are obtained:

$$\int_{\Omega} \nabla^s \mathbf{w}^T \, \mathbf{C} \, \nabla^s \mathbf{u} \, d\Omega = \int_{\Omega} \mathbf{w}^T \, \mathbf{b} \, d\Omega + \int_{\Gamma} \mathbf{w}^T \, \mathbf{t} \, d\Gamma, \tag{4}$$

where $\mathbf{C}$ is the constitutive relationship tensor and $\nabla^s(\cdot)$ is the symmetrical part of tensor $\nabla(\cdot)$, and can be defined as:

$$\nabla^s(\cdot) = \frac{1}{2}\left(\nabla(\cdot) + \nabla(\cdot)^T\right). \tag{5}$$

Now, using the domain, $\mathbf{\Psi}(\mathbf{x})$, and boundary, $\mathbf{\Phi}(\mathbf{x})$, shape functions, the domain and boundary fields are described as:

$$\tilde{\mathbf{u}}(\mathbf{x}) = \begin{bmatrix} \mathbf{\Psi}(\mathbf{x}) & \mathbf{0} \\ \mathbf{0} & \mathbf{\Psi}(\mathbf{x}) \end{bmatrix} \mathbf{u}_{\mathrm{D}}, \tag{6}$$

$$\tilde{\mathbf{b}}(\mathbf{x}) = \begin{bmatrix} \mathbf{\Psi}(\mathbf{x}) & \mathbf{0} \\ \mathbf{0} & \mathbf{\Psi}(\mathbf{x}) \end{bmatrix} \mathbf{b}_{\mathrm{D}}, \tag{7}$$

and

$$\tilde{\mathbf{t}}(\mathbf{x}) = \begin{bmatrix} \mathbf{\Phi}(\mathbf{x}) & \mathbf{0} \\ \mathbf{0} & \mathbf{\Phi}(\mathbf{x}) \end{bmatrix} \mathbf{t}_{\mathrm{B}}, \tag{8}$$

where $\mathbf{x} \in \mathbb{R}^2$, $\mathbf{u}_{\mathrm{D}}$, $\mathbf{t}_{\mathrm{B}}$ and $\mathbf{b}_{\mathrm{D}}$ are the vector with nodal values of $\mathbf{u}$, $\mathbf{t}$ and $\mathbf{b}$, respectively.

The domain shape functions $\mathbf{\Psi}(\mathbf{x})$ are the Finite Element Method shape functions, and the boundary shape functions $\mathbf{\Phi}(\mathbf{x})$ need to respect the trace property, in other words:

$$\mathbf{\Phi}(\mathbf{x}) = \lim_{\mathbf{x}\to\Gamma} \mathbf{\Psi}(\mathbf{x}), \tag{9}$$

or as represented in Fig. 1. The enrichment shape functions are constructed as in the GFEM, as describe in next section.

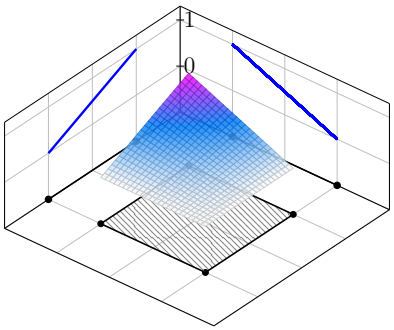

Figure 1: Representation of the domain and the boundary shape functions.

The main difference between this method and the FEM is that the first one does not require that the weight functions are null in the Dirichlet boundary, as the FEM. Since the weight functions are not null, it is necessary to define an approximation for the tractions in all boundary by Eq. (8). Using this approximation, and the ones in Eq. (6) and (7), and using the same basis functions as weight functions $\mathbf{w}$, the Eq. (4) can be rewritten as:

$$\mathbf{K}\,\mathbf{u}_{\mathrm{D}} = \mathbf{D}\,\mathbf{t}_{\mathrm{B}} + \mathbf{A}\,\mathbf{b}_{\mathrm{D}}, \tag{10}$$

where $\mathbf{K}$ is the same stiffness matrix as the FEM, $\mathbf{D}$ is the matrix of the inner dot product on the boundary shape functions, and $\mathbf{A}$ is the matrix of the inner dot product on the domain shape functions.

The Green's functions are not required to be obtained in this approach, they are implicit in the formulation and can be defined as (Corrêa *et al.*, 2023):

$$\mathbf{K}\,\mathbf{G}^{\mathrm{DQ}} = \mathbf{A} \quad \text{or} \quad \mathbf{G}^{\mathrm{DQ}} = \mathbf{K}^{-1}\,\mathbf{A}; \tag{11a}$$

$$\mathbf{K}\,\mathbf{G}^{\mathrm{BQ}} = \mathbf{D} \quad \text{or} \quad \mathbf{G}^{\mathrm{BQ}} = \mathbf{K}^{-1}\,\mathbf{D}; \tag{11b}$$

where $\mathbf{G}^{\mathrm{DQ}}$ and $\mathbf{G}^{\mathrm{BQ}}$ are the nodal values of the Green's functions projections when the source is on the domain and on the boundary, respectively. More details about these projections can be found in Barbieri *et al.* (1998).

The system in Eq. (10) can be solved by imposing the boundary conditions in a similar way to the BEM, switching columns of $\mathbf{K}$ and $\mathbf{B}$ related to the prescribed boundary conditions as:

$$[-\mathbf{D} \quad | \quad \mathbf{K}] \left\{ \begin{array}{c} \mathbf{t}_{\mathrm{B}} \\ \mathbf{u}_{\mathrm{D}} \end{array} \right\} = \left[-\bar{\mathbf{K}} \quad | \quad \bar{\mathbf{D}}\right] \left\{ \begin{array}{c} \bar{\mathbf{u}}_{\mathrm{D}} \\ \bar{\mathbf{t}}_{\mathrm{B}} \end{array} \right\} + \mathbf{A}\, \mathbf{b}_{\mathrm{D}}, \tag{12}$$

where $\bar{\mathbf{u}}_{\mathrm{D}}$ and $\bar{\mathbf{t}}_{\mathrm{B}}$ are the prescribed displacements and tractions in the boundary.

3. THE GENERALIZED FINITE ELEMENT METHOD

The Generalized Finite Element Method can be described as the combination of the FEM with the Partition of Unity Method. The stable version of the GFEM (Babuška and Banerjee, 2012) describes the approximation of the displacement field $\mathbf{u}$ as follows:

$$\tilde{u}^{(k)}(\mathbf{x}) = \sum_{j=1}^{n} \mathcal{N}_j(\mathbf{x}) \left[u_j^{(k)} + \sum_{i=1}^{q_j} \left\{ \mathcal{L}_{ji}(\mathbf{x}) - \mathcal{I}_{\Omega_j}(\mathcal{L}_{ji})(\mathbf{x}) \right\} a_{ji}^{(k)} \right], \tag{13}$$

where n is the number of nodes in mesh, $\mathcal{N}_j(\mathbf{x})$ is the partition of unity function, $a_{ji}^{(k)}$ are the GFEM nodal degrees of freedom in the k direction, $\mathcal{L}_{ji}(\mathbf{x})$ are the enrichment functions related to node j, q_j is the number of enrichment functions related to node j, and $\mathcal{I}_{\Omega_j}(\mathcal{L}_{ji})(\mathbf{x})$ is the piecewise linear interpolant of $\mathcal{L}_{ji}$ on path Ω_j.

In this paper, the linear Lagrangian finite element shape functions are used as the partition of unity functions. The numerical simulations present two types of enrichments, one to introduce the displacement discontinuous in the crack path and another to represent the singularity on the crack tip.

The discontinuous is introduced using the linearized Heaviside functions and are written as:

$$\bar{\boldsymbol{\mathcal{H}}}_j(\mathbf{x}) = \left\{ \mathcal{H}(\mathbf{x}), \mathcal{H}(\mathbf{x}) \left(\frac{x^{(1)} - x_j^{(1)}}{h_j} \right), \mathcal{H}(\mathbf{x}) \left(\frac{x^{(2)} - x_j^{(2)}}{h_j} \right) \right\}, \tag{14}$$

where $\left(x^{(1)}, x^{(2)}\right)$ are the coordinates of $\mathbf{x}$, $\left(x_j^{(1)}, x_j^{(2)}\right)$ are the coordinates of node $\mathbf{x}_j$, h_j is a scaling factor given by the diameter of the largest element in the support of node $\mathbf{x}_j$, and $\mathcal{H}(\mathbf{x})$ is defined as:

$$\mathcal{H}(\mathbf{x}) = \left\{ \begin{array}{rcl} 1 & \forall & \xi > 0 \\ -1 & \forall & \xi < 0 \end{array} \right. , \tag{15}$$

where ξ denotes the relative position of the discontinuity assumed at $\xi = 0$. The crack tip enrichment functions are defined as:

$$\boldsymbol{\mathcal{S}}(r, \theta) = \left\{ \sqrt{r} \cos\frac{\theta}{2}, \sqrt{r} \sin\frac{\theta}{2}, \sqrt{r} \cos\frac{\theta}{2} \sin\theta, \sqrt{r} \sin\frac{\theta}{2} \sin\theta \right\}, \tag{16}$$

where r and θ are coordinates of the polar system centered at the crack tip.

4. NUMERICAL RESULTS

In this section, two stress plane state problems are analyzed. The two problems can be equated as follows:

$$\nabla \cdot \boldsymbol{\sigma} = \mathbf{0} \quad \text{in} \quad \Omega, \tag{17}$$

with the following boundary conditions:

$$\mathbf{u} = \bar{\mathbf{u}} \quad \text{in} \quad \Gamma_{\mathrm{D}}, \tag{18}$$

$$\boldsymbol{\sigma} \cdot \mathbf{n} = \bar{\mathbf{t}} \quad \text{in} \quad \Gamma_{\mathrm{N}}, \tag{19}$$

$$\boldsymbol{\sigma} \cdot \mathbf{n} = \mathbf{0} \quad \text{in} \quad \Gamma_{\mathrm{c}}^{+} \text{ and } \Gamma_{\mathrm{c}}^{-}, \tag{20}$$

and the models thickness are $h = 0.1$ m.

The manufactured solution was obtained through the first term of mode I expansion of the elasticity solution in the neighborhood of a crack tip. The boundary conditions are applied from analytical expressions of the displacement fields and stresses, presented as follows (Szabó and Babuška, 2021):

$$u_x(r, \theta) = \frac{1}{2\mu} \sqrt{\frac{r}{2\pi}} \cos\frac{\theta}{2} \left(\kappa - 1 + 2\sin^2\frac{\theta}{2} \right), \tag{21}$$

$$u_y(r,\theta) = \frac{1}{2\mu}\sqrt{\frac{r}{2\pi}}\sin\frac{\theta}{2}\left(\kappa + 1 - 2\cos^2\frac{\theta}{2}\right), \tag{22}$$

$$\sigma_{xx}(r,\theta) = \frac{1}{\sqrt{2\pi r}}\cos\frac{\theta}{2}\left(1 - \sin\frac{\theta}{2}\sin\frac{3\theta}{2}\right), \tag{23}$$

$$\sigma_{yy}(r,\theta) = \frac{1}{\sqrt{2\pi r}}\cos\frac{\theta}{2}\left(1 + \sin\frac{\theta}{2}\sin\frac{3\theta}{2}\right), \tag{24}$$

and

$$\tau_{xy}(r,\theta) = \frac{1}{\sqrt{2\pi r}}\cos\frac{\theta}{2}\sin\frac{\theta}{2}\cos\frac{3\theta}{2}, \tag{25}$$

where $\mu = \dfrac{E}{2(1+\nu)}$, $\kappa = \dfrac{3-\nu}{1+\nu}$, E is the Young's modulus and ν is the Poisson's ratio. The Young's modulus is assumed to be 200(10^3) MPa, and the Poisson's ratio is assumed to be 0.3.

4.1 HORIZONTAL CRACK MODEL

The first example is a horizontal crack as the scheme in Fig. 2. The initial meshes in the analyses are presented in Fig. 3. The ratio around the crack tip with the value of 0.145 m is enriched with the crack tip functions defined in Eq. (16), and this ratio is constant for all mesh refinements. The nodes of the elements out of this ratio and divided by the crack are enriched with the linearized Heaviside functions presented in Eq. (14).

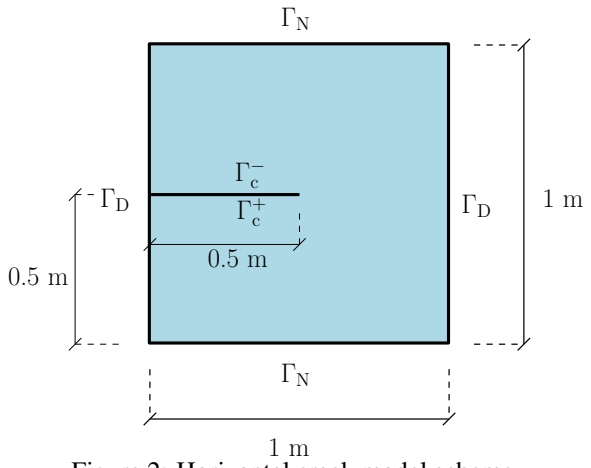

Figure 2: Horizontal crack model scheme.

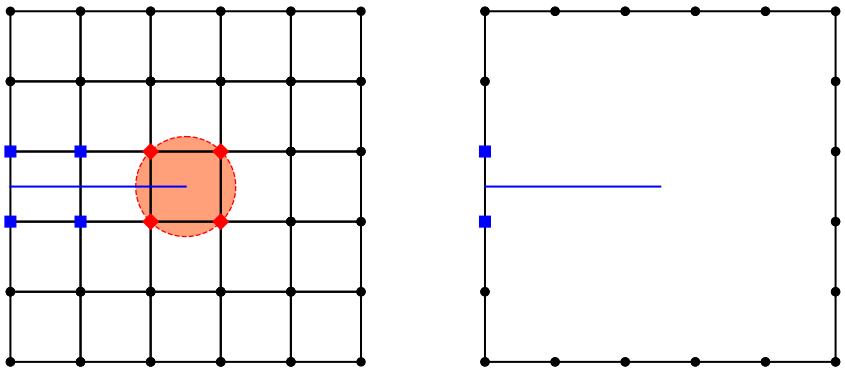

(a) (b)

Figure 3: Initial meshes: (a) domain and (b) boundary. Nodes with ◆ markers are enriched with crack tip functions defined in Eq. (16) and nodes with ■ markers are enriched with the Heaviside functions defined in Eq. (14).

The first results are presented in Fig. 4, where it is shown the convergence of the displacement for the enriched ML-GFM and the GFEM. The results are expressed in terms of the L_2-error norm. It can be seen that the GFEM displacement results are more precise than enriched MLGFM ones. The GFEM convergence is also more stable, having a constant rate.

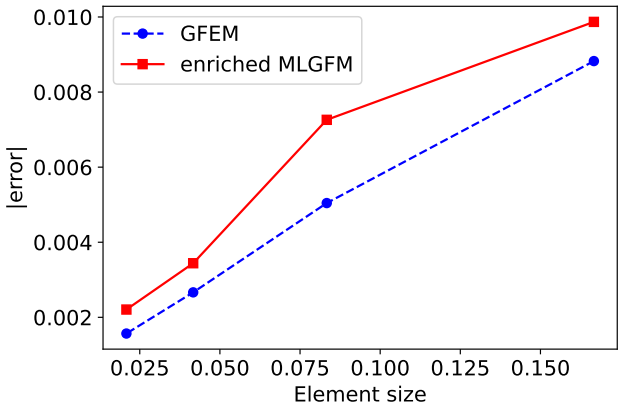

Figure 4: Displacement convergence of enriched MLGFM and GFEM for horizontal crack.

The second result is the σ_x stress component at the right boundary ($x = 1$) for the initial mesh of the enriched MLGFM and the GFEM, as presented in Fig. 5. As can be seen, the enriched MLGFM σ_x stress results are more similar to the analytical results than the GFEM ones, even for a poor mesh. This result reinforces one of the main features of the enriched MLGFM, that is the superconvergence of stress in the boundary.

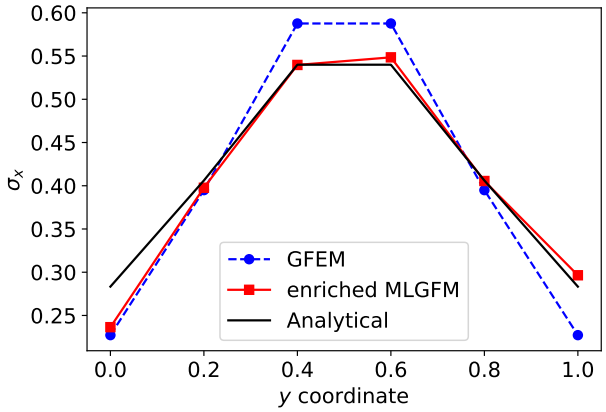

Figure 5: σ_x stress component obtained by enriched MLGFM and GFEM for the initial mesh, at $x = 1$.

The third result is the τ_{xy} stress component at the right boundary ($x = 1$) for the initial mesh of the enriched MLGFM and the GFEM, as presented in Fig. 6. For this stress component, unlike what was observed in previous works, the GFEM results are more precise than enriched MLGFM ones. This can be explained by the ill-conditioning introduced in the enriched MLGFM formulation by the enrichment functions.

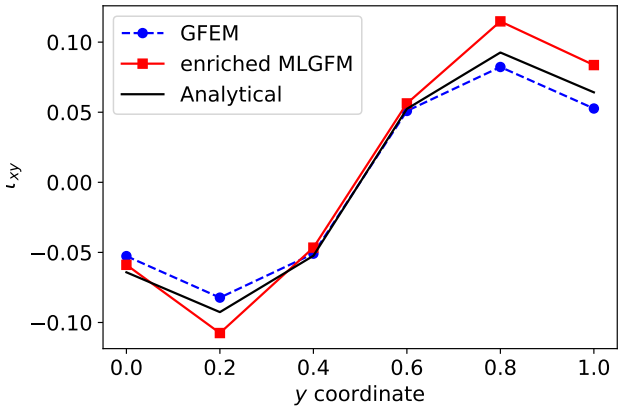

Figure 6: τ_{xy} stress component obtained by enriched MLGFM and GFEM for the initial mesh, at $x = 1$.

4.2 INCLINED CRACK MODEL

The second example is a model with a crack angle $\theta = 29.82^o$ as shown in Fig. 7. The initial meshes used in this model are presented in Fig. 8. The region enriched with the functions defined in Eq. (16) has the same ratio as the previous example. Once again, the nodes of the elements out of this ratio and divided by the crack are enriched with the linearized Heaviside functions presented in Eq. (14).

The displacement convergence using the L_2-error norm is presented in Fig. 9. As observed in the previous model, the displacements obtained by the GFEM are more precise than the enriched MLGFM ones. The convergence rates are similar for both models.

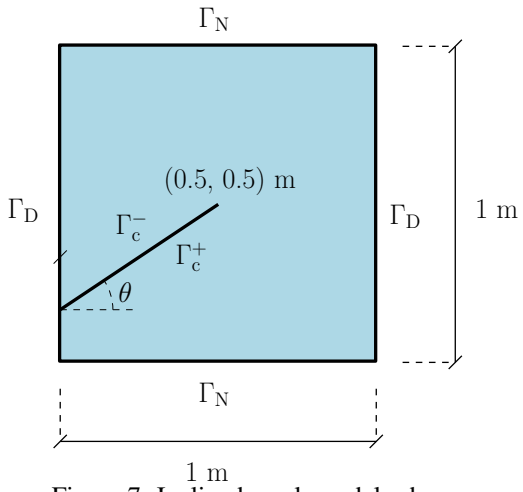

Figure 7: Inclined crack model scheme.

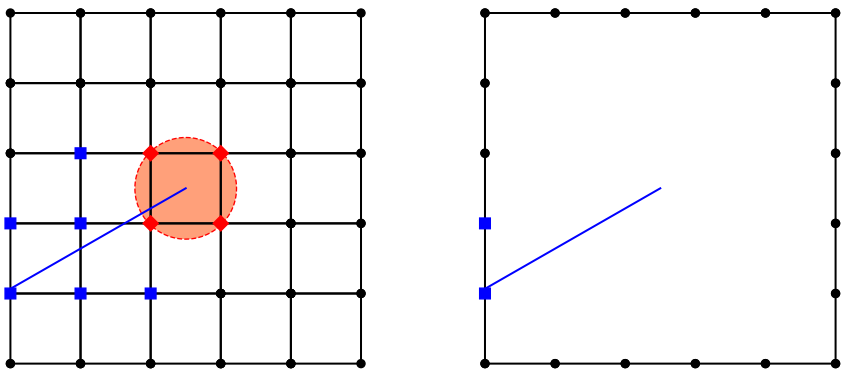

(a) (b)

Figure 8: Initial meshes: (a) domain and (b) boundary. Nodes with ◆ markers are enriched with crack tip functions defined in Eq. (16), and nodes with ■ markers are enriched with the Heaviside functions defined in Eq. (14).

The σ_x stress component results at $x = 1$ for the initial meshes are presented in Fig. 10. As in example 1, the stress results for the enriched MLGFM are more precise than GFEM ones, even for this coarse mesh. As expected, the results obtained by the enriched MLGFM for the boundary stress are more accurate than the GFEM ones.

The τ_{xy} stress component results at $x = 1$ for the initial meshes are presented in Fig. 11. As in example 1, these component stress results obtained by the GFEM are more precise than the enriched MLGFM ones. Once again, this can be explained by the ill-conditioning introduced by the enrichment of the enriched MLGFM formulation.

5. CONCLUDING REMARKS

This paper presents an enriched version of the MLGFM applied to static cracks. In the two analyzed examples, the GFEM presents more accurate results for displacements, as shown in Figs. 4 and 9. The σ_x stress components obtained directly from the tractions are more precise in enriched MLGFM than in GFEM, even for coarse meshes, as shown in Figs. 5 and 10. The good approximation of the tractions is one of the main features of the MLGFM formulation as demonstrated in several previous studies. The MLGFM obtains an approximation of the tractions directly from the solution of the system

of equations, without the need for post-processing. Therefore, these results are often more accurate than those obtained by other methods that require post-processing.

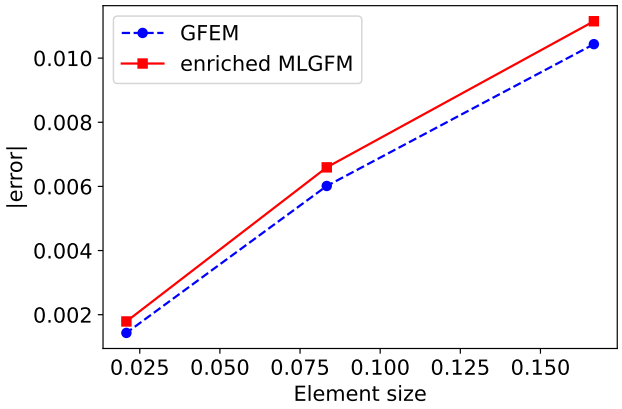

Figure 9: Displacement convergence of enriched MLGFM and GFEM for inclined crack.

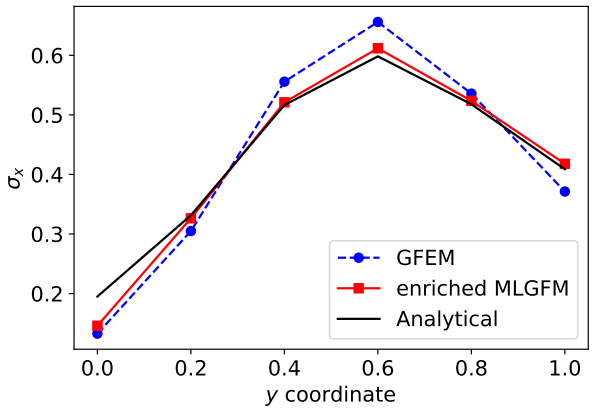

Figure 10: σ_x stress component obtained by enriched MLGFM and GFEM for the initial mesh, at $x = 1$, for inclined crack.

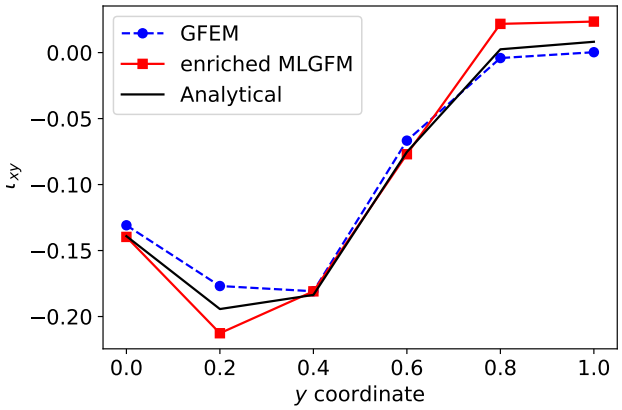

Figure 11: τ_{xy} stress component obtained by enriched MLGFM and GFEM for the initial mesh, at $x = 1$, for inclined crack.

Although in both cases the τ_{xy} stress components obtained by the GFEM were more accurate than the enriched MLGFM ones for the initial mesh, this can be the result of the ill-conditioning brought to the enriched MLGFM formulation by the enrichment technique. Another benefit bring for this enriched MLGFM is to avoid the need of an explicit representation of the crack. In the regular MLGFM the boundary in the crack needs to be explicitly represented in the boundary and domain meshes. So, although the enriched MLGFM still needs further development, the results show that the use of

this enriched method deserves to be further studied for this type of problem, especially when the tractions are important for the analysis.

6. ACKNOWLEDGEMENTS

The authors gratefully acknowledge CAPES (grant number: 88887.825830/2023-00) and CNPq (grant numbers: 301802/2022-0 and 316985/2021-0) for their financial support. The authors also acknowledge the PPGEC (Graduated Program in Civil Engineering) and the UFPR (Federal University of Paraná) for their institutional support.

7. REFERENCES

Babuška, I. and Banerjee, J., 2012. "Stable generalized finite element method (SGFEM)". *Computer Methods in Applied Mechanics and Engineering*, Vol. 201-204, pp. 91–111. doi:10.1016/j.cma.2011.09.012.

Babuška, I., Caloz, G. and Osborn, J.E., 1994. "Special finite element methods for a class of second order elliptic problems with rough coefficients". *SIAM Journal on Numerical Analysis*, Vol. 31, p. 945–981. doi:10.1137/0731051.

Barbieri, R. and Barcellos, C.S., 1993a. "Mindlin's plate solutions by the mlgfm". In C.A. Brebbia and J.J. Rencis, eds., *Boundary Elements XV*, Computational Mechanics Publications, Southampton, Vol. 2, pp. 149–164.

Barbieri, R. and Barcellos, C.S., 1993b. "Non-homogeneous field potential problems solution by the modified local Green's function method (MLGFM)". *Engineering Analysis with Boundary Elements*, Vol. 11, No. 1, pp. 9–15. doi: 10.1016/0955-7997(93)90073-t.

Barbieri, R. and Machado, R.D., 2015. "The local formulation for the modified Green's function method". *Latin American Journal of Solids and Structures*, Vol. 12, No. 5, pp. 883–904. doi:10.1590/1679-78251281.

Barbieri, R. and Muñoz, P.A.R., 1998. "Modified local green's function method (MLGFM) part II. application for accurate flux and traction evaluation". *Engineering Analysis with Boundary Elements*, Vol. 22, No. 2, pp. 153–159. doi: 10.1016/S0955-7997(97)00110-0.

Barbieri, R., Muñoz, P.A.R. and Machado, R.D., 1998. "Modified local Green's function method (MLGFM) part I. mathematical background and formulation". *Engineering Analysis with Boundary Elements*, Vol. 22, No. 2, pp. 141–151. doi:10.1016/S0955-7997(97)00109-4.

Barcellos, C.S. and Silva, L.H.M., 1987. "Elastic membrane solution by a modified local Green's function method". In C.A. Brebbia and C.S. Venturine, eds., *Proceedings of the international conference on boundary element technology*. Computational Mechanics Publications, Southampton.

Bathe, K., 1996. *Finite Element Procedures in Engineering Analysis*. Prentice-Hall, New Jersey.

Brebbia, C.A. and Dominguez, J., 1992. *Boundary Elements: an introductory course*. WIT Press/Computational Mechanics Publications.

Brebbia, C.A., Telles, J.C.F. and Wrobel, L.C., 1984. *Boundary Element Techniques: Theory and Applications in Engineering*. Springer-Verlag Berlin Heidelberg, 1st edition. ISBN 978-3-642-48862-7,978-3-642-48860-3.

Burns, T.J., 1975. *The Partial Current Balance Method: A Local Green's Function Technique for the Numerical Solution of Multidimensional Neutron Diffusion Problems*. Phd thesis, University of Illinois at Urbana-Champaign.

Corrêa, R.M., Arndt, M. and Machado, R.D., 2023. "A new approach for the Modified Local Green's Function Method applied to solid mechanics problems". *Engineering Analysis with Boundary Elements*, Vol. 155, pp. 907–919. doi: 10.1016/j.enganabound.2023.07.009.

Dolbow, J., Moës, N. and Belytschko, T., 2000. "Modeling fracture in mindlin–reissner plates with the extended finite element method". *International Journal of Solids and Structures*, Vol. 37, No. 48-50, pp. 7161–7183. doi:10.1016/s0020-7683(00)00194-3.

Gupta, P., Pereira, J.P., Kim, D.J., Duarte, C.A. and Eason, T., 2012. "Analysis of three-dimensional fracture mechanics problems: A non-intrusive approach using a generalized finite element method". *Engineering Fracture Mechanics*, Vol. 90, pp. 41–64. doi:10.1016/j.engfracmech.2012.04.014.

Horak, W.C., 1980. *Local Green's Function Techniques for the Solution of Heat Conduction and Incompressible Fluid Flow Problems*. Phd thesis, University of Illinois at Urbana-Champaign.

Horak, W.C. and Dorning, J.J., 1977. "A local Green's function method for the numerical solution of heat conduction and fluid flow problems". *Nuclear Science and Engineering*, Vol. 64, No. 1, pp. 192–207. doi:10.13182/nse77-a27090.

Kim, D.J., Duarte, C.A. and Sobh, N.A., 2011. "Parallel simulations of three-dimensional cracks using the generalized finite element method". *Computational Mechanics*, Vol. 47, No. 3, pp. 265–282. doi:10.1007/s00466-010-0546-5.

Machado, R.D., Abdalla Filho, J.E. and Silva, M.P., 2008. "Stiffness loss of laminated composite plates with distributed damage by the modified local Green's function method". *Composite Structures*, Vol. 84, No. 3, pp. 220–227. doi: 10.1016/j.compstruct.2007.08.001.

Machado, R.D., Barbieri, R., Filippin, C.G. and Barcellos, C.S., 1994. "Comparative analysis of the finite element method with the modified local Green's function method for application to the solution of composite laminated plates". *Revista Brasileira de Ciências Mecânicas*, Vol. 16, No. 1, pp. 27–34.

Melenk, J.M., 1995. *On generalized finite element methods*. (phd thesis, University of Maryland, College Park.

Rivadeneira, A.G.S. and Duarte, C.A., 2019. "A stable generalized/eXtended FEM with discontinuous interpolants for fracture mechanics". *Computer Methods in Applied Mechanics and Engineering*, Vol. 345, pp. 876–918. doi: 10.1016/j.cma.2018.11.018.

Szabó, B. and Babuška, I., 2021. *Finite Element Analysis: Method, Verification and Validation*. John Wiley & Sons. ISBN 978-1-119-42642-4.

Zienkiewicz, O.C., Taylor, R.L. and Zhu, J.Z., 2005. *The Finite Element Method: Its Basis and Fundamentals*. Butterworth-Heinemann, 6th edition. ISBN 0750663200,9780750663205.

8. RESPONSIBILITY NOTICE

The authors are solely responsible for the printed material included in this paper.